Synthesis and preclinical evaluation of [C-11]LR111 and [F-18]EW-7197 as PET tracers of the activin-receptor like kinase-5

Rotteveel, L.; Kurakula, K.; Kooijman, E.J.M.; Schuit, R.C.; Verlaan, M.; Schreurs, M.; ... ; Windhorst, A.D.

Nuclear Medicine and Biology 112-113 (2022) 9–19

Contents lists available at ScienceDirect

Nuclear Medicine and Biology

journal homepage: www.elsevier.com/locate/nucmedbio

Synthesis and preclinical evaluation of [^{11}C]LR111 and [^{18}F]EW-7197 as PET tracers of the activin-receptor like kinase-5

Lonneke Rotteveel [a,*], Kondababu Kurakula [c], Esther J.M. Kooijman [a], Robert C. Schuit [a], Mariska Verlaan [a], Maxime Schreurs [a], Wissam Beaino [a], Maarten A.H. van Dinther [d], Peter ten Dijke [d], Adriaan A. Lammertsma [a], Alex J. Poot [a], Harm Jan Bogaard [b], Albert D. Windhorst [a,1]

[a] Amsterdam UMC, VU University Medical Center, Radiology & Nuclear Medicine (Amsterdam Cardiovascular Sciences), de Boelelaan 1085c, Amsterdam, the Netherlands
[b] Amsterdam UMC, VU University Medical Center, Pulmonary Medicine (Amsterdam Cardiovascular Sciences), de Boelelaan 1117, Amsterdam, the Netherlands
[c] Leiden University Medical Center, Dept. Cell and Chemical Biology, Einthovenweg 20, the Netherlands
[d] Oncode Institute and Leiden University Medical Center, Dept. Cell and Chemical Biology, Einthovenweg 20, the Netherlands

ARTICLE INFO

Keywords:
TGFβ type I receptor
Positron emission tomography
Cancer
MDA-MB-231 tumour xenografts

ABSTRACT

The transforming growth factor β (TGFβ) pathway plays a complex role in cancer biology, being involved in both tumour suppression as well as promotion. Overactive TGFβ signalling has been linked to multiple diseases, including cancer, pulmonary arterial hypertension, and fibrosis. One of the key meditators within this pathway is the TGFβ type I receptor, also termed activin receptor-like kinase 5 (ALK5). ALK5 expression level is a key determinant of TGFβ signalling intensity and duration, and perturbation has been linked to diseases. A validated ALK5 positron emission tomography (PET) tracer creates an opportunity, therefore, to study its role in human diseases. To develop ALK5 PET tracers, two small molecule ALK5 kinase inhibitors were selected as lead compounds, which were labelled with carbon-11 and fluorine-18, respectively. [^{11}C]LR111 was synthesized with a yield of 17 ± 6%, a molar activity of 126 ± 79 GBq·μmol^{-1} and a purity of >95% (n = 44). [^{18}F]EW-7197 was synthesized with a yield of 10 ± 5%, a molar activity of 183 ± 126 GBq·μmol^{-1} and a purity of >95% (n = 11). Metabolic stability was evaluated *in vivo* in mice, showing 39 ± 2% of intact [^{11}C]LR111 and 21 ± 2% of intact [^{18}F]EW-7197 in blood plasma at 45 min p.i. *In vitro* binding experiments were conducted in breast cancer MDA-MB-231 and lung cancer A431 cell lines. In addition, both tracers were used for PET imaging in MDA-MB-231 xenograft models. Selective uptake of [^{18}F]EW-7197 and [^{11}C]LR111 was observed in MDA-MB-231 cells, in the MDA-MB-231 tumour xenografts *in vivo* and in the autoradiograms. As [^{11}C]LR111 and [^{18}F]EW-7197 showed selectivity of binding to ALK5 *in vivo* and *in vitro*. Both tracers are thereby valuable tools for the detection of ALK5 activity.

1. Introduction

The transforming growth factor β (TGFβ) family of cytokines regulates embryonic development, and physiological and cellular processes [1]. TGFβ plays a complex role in cancer biology. In the early stage of tumour development, it acts as a tumour suppressor, but during further tumour development the expression of TGFβ is increased and cancer cells become resistant to its cytostatic effects. Furthermore, TGFβ acts on the tumour microenvironment to make it conducive to rapid tumour growth and metastasis development [2–5].

TGFβ exerts its cellular effects by inducing the formation of heteromeric complexes of TGFβ type II (TβRII) and TGFβ type I (TβRI) receptors, also known as activin receptor-like kinase 5 (ALK5). Upon phosphorylation by TβRII kinase, activated ALK5 phosphorylates downstream enzymes SMAD2 and SMAD3, which can form heteromeric complexes with SMAD4. These activated SMAD complexes can

* Corresponding author at: Department of Radiology & Nuclear Medicine, Amsterdam UMC, VU University Medical Center, De Boelelaan 1085c, 1081 HV Amsterdam, the Netherlands.
E-mail address: l.rotteveel@amsterdamumc.nl (L. Rotteveel).
[1] Given his role as Editor, A.D. Windhorst had no involvement in the peer-review of this article and has no access to information regarding its peer-review

https://doi.org/10.1016/j.nucmedbio.2022.05.003
Received 23 February 2022; Received in revised form 12 May 2022; Accepted 19 May 2022
Available online 24 May 2022

translocate into the nucleus, where they can act as transcription factors and induce alterations in specific gene expressions [6]. Elevated levels of the TβRI and increased signalling were found in numerous diseases such as pulmonary arterial hypertension, temporal lobe epilepsy, colonic fibrosis, pancreatic cancer, and breast cancer [7–11].

Positron emission tomography (PET) using tracers of the TGFβ pathway, and more specifically ALK5, could provide a non-invasive way to evaluate its expression *in vivo*, thereby enabling better understanding of its role in diseases like cancer. Furthermore, radiolabelled ALK5 tracers could be used to support drug development and clinical research and improve patient care [12]. To date, no ALK5 PET tracers have been developed to assess its expression *in vivo* even though it is widely involved in multiple diseases. Therefore, two ALK5 targeting PET tracers based upon selective kinase inhibitors were developed and evaluated both *in vitro* and *in vivo* in breast and lung cancer models. Inspired by an ALK5 binder described by Amada et al. et al. [13], which displayed a desirable profile with respect to the half maximal inhibitory concentration (IC_{50}) of 5.5 nM and selectivity being more than 200 fold higher for ALK5 than for 96 other kinases, [^{11}C]LR111 was developed. Next, a fluorine-18 labelled tracer, [^{18}F]EW-7197, was developed based on an ALK5 binder described by Jin et al. [14]. EW-7197 displayed an IC_{50} value of 13 nM and a K_i value of 21 nM with 176-fold higher selectivity for ALK5 over a panel of 320 other kinases [15]. Both [^{11}C]LR111 and [^{18}F]EW-7197 bind to the ATP-binding site of ALK5, which is located intracellularly. Upon binding of both inhibitors to the ATP-binding site, ATP is competitively displaced from the active site, interrupting downstream signalling. The kinase domains of ALK4, ALK5 and ALK7 are quite similar [16]. Therefore, [^{11}C]LR111 and [^{18}F]EW-7197 will also bind to ALK4 and ALK7 with a similar potency. After synthesis, the new tracers were extensively evaluated in ALK5 expressing *in vitro* and *in vivo* models.

2. Materials and methods

2.1. General information

Chemicals and solvents were obtained from Sigma Aldrich (Sigma-Aldrich, St. Louis, MO) and Biosolve (Valkenswaard, The Netherlands), respectively, unless otherwise mentioned, and were used as received without further purification. Analytical HPLC was performed on a Jasco PU-1580 pump (Easton, USA), a Jasco UV-2075 detector (λ = 254 nm) and a NaI radioactivity detector (Raytest, Straubenhardt, Germany). Chromatograms were acquired using GINA star software (version 5.8, Raytest). Semi-preparative HPLC was carried out on a Jasco PU-2089 pump (Easton, MD, USA), a Jasco UV1575 detector (λ = 254 nm) and a custom-made radioactivity detector. Chromatograms were acquired using ChromNAV software (version 1.14.01, Jasco). A Wizard 2480 gamma well counter (Perkin-Elmer, Groningen, The Netherlands) was used for γ-counting. Animal experiments were performed in accordance with the European Community Council Directive (2010/63/EU) for laboratory animal care and the Dutch Law on animal experimentation. The experimental protocol was validated and approved by the central committee for animal experimentation (CCD) and the local committee on animal experimentation of the Amsterdam University Medical Center, location VUmc. Female SCID mice (8 weeks at arrival, 20–25 g, Charles River, Sulzfeld, Germany) were group housed with a maximum of 6 mice per cage under standard conditions (20–24 °C, 50–70% relative humidity, 12-h light/dark cycles), provided with nesting material, sawdust, sterile water and food (Teklad Global 16% Protein Rodent Diet, Harlan, Madison, WI, USA). Fractions from the metabolite analysis were counted for radioactivity in a compugamma (Wallac 1210 Compugamma, Turku, Finland). Online HPLC analysis during metabolite analysis was performed on a Dionex (Sunnyvale, CA, USA) UltiMate 3000 HPLC with Chromeleon software (version 6.8).

LC-MS/MS analysis was performed on a Jasco X-LC system (Easton, PA, USA) equipped with an QTRAP 5500 mass spectrometer (AB Sciex, Ontario, Canada) and an Analyst 1.5.1 turbo ionization spray (AB Sciex, Ontario, Canada). The Jasco system consisted of two pumps (X-LC 3180PU), a degasser (X-LC 3080DG), a mixer (X-LC 3080MX), a column oven (X-LC 3161CO), an autosampler (X-LC3159AS) and an ultraviolet (UV) detector at 232 nm (X-LC 3075UV). Data were analysed using Analyst 1.0.56 software (AB Sciex, Ontario, Canada). A Phenomenex Kinetex biphenyl (2.6 μm, 100 A, 2.1 × 100 mm) column (Torrance, CA, USA) was used for chromatographic separation.

2.2. Radiosynthesis of [^{11}C]LR111

Precursor **6** (Scheme 1) and LR111 were synthesized according to Amada et al. [13]. Detailed experimental procedures are described in the Supplementary data. [^{11}C]CO_2 was produced by the ^{14}N (p,α)^{11}C nuclear reaction performed in a 0.5% O_2/N_2 gas mixture using an IBA Cyclone 18/9 cyclotron (IBA, Louvain-la-Neuve, Belgium). Radiochemistry was performed using a synthesis module build in-house, equipped with a VIK-202 ionization-chamber (Comecer, Joure, The Netherlands) [17]. A reaction vial was purged with helium, charged with 2-tert-butylimino-2-diethylamino-1,3-dimethylperhydro-1,3,2-diazaphosphorine (BEMP) (8.3 μL, 7.9 mg, 29 μmol) and precursor **6** (0.5 mg, 1.6 μmol) in 200 μL dimethyl sulfoxide (DMSO) obtained from Fisher Scientific (Hampton, United States). The vessel was bubbled through with helium (25 mL·min^{-1}) for 3 min before [^{11}C]CO_2 was transferred to the reaction vessel at 25 °C until the trapped amount of radioactivity was constant (~2 min). Next, 1-iodo-2-methylpropane (3.5 μL, 5.6 mg, 30 μmol) in DMSO (100 μL) was added. This reaction mixture was heated at 75 °C for 10 min after which 1 mL of HPLC-eluent was added and the complete mixture injected onto the Luna C18 5 μm (10 × 250 mm) column (Phenomenex, Utrecht, The Netherlands) using a mixture of (4 mM of sodium formate in water and 4% DMF)/MeCN (6/4, HPLC, v/v) as eluent with a flow rate of 8 mL·min^{-1}. The collected fraction was diluted with 40 mL of sterile water and passed over a C18 SepPak cartridge (Waters, Etten-Leur, The Netherlands), which was preconditioned with 10 mL of ethanol and then with 10 mL of water. Next, the cartridge was washed with 20 mL sterile water after which the product was eluted from the cartridge with 1.0 mL of sterile 96% ethanol. The ethanol was diluted to 10 vol% with the formulation solution (7.09 mM NaH_2PO_4 in 0.9% NaCl, w/v in water, pH 5.2) into a sterile 20 mL capped vial (ABX, Radeberg, Germany). Analytical HPLC was performed with an X-bridge: C-18 5 μm (4.6 × 100 mm) column (Waters, Etten-Leur, The Netherlands) using water/MeCN (7/3, HPLC, v/v) + 0.1% TFA as mobile phase at a flow rate of 1 mL·min^{-1}, retention time (t_R) = 5.5 min.

2.3. Radiosynthesis of [^{18}F]EW-7197

[^{18}F]fluoride was produced by the ^{18}O (p,n)^{18}F nuclear reaction performed in ^{18}O enriched water using an IBA Cyclone 18/9 cyclotron (IBA, Louvain-la-Neuve, Belgium). After target irradiation, the [^{18}F]fluoride was trapped on a preconditioned PS-HCO_3 column (ABX, Radenberg, Germany). Preconditioning was performed with 1 mL EtOH and 4 mL water. Elution of [^{18}F]fluoride from the PS-HCO_3 column into a 3 mL screw-cap reaction vessel was performed with 1 mL MeCN/water (9/1, v/v) containing Kryptofix$_{2.2.2.}$ (13 mg, 35 μmol) and K_2CO_3 (2.0 mg, 15 μmol). The fluorine-18 solution was dried by azeotropic distillation at 90 °C with a helium flow of 50 mL·min^{-1} under vacuum until dryness. Next, 0.5 mL of MeCN (VWR, Radnor, United States) was added and evaporated at 90 °C with a helium flow of 50 mL·min^{-1} under vacuum. The dried residue was dissolved in dry MeCN (0.5 mL) (VWR, Radnor, United States) containing 1,2-dinitrobenzene (0.5 mg, 3.0 μmol). The reaction mixture was heated to 130 °C and reacted for 10 min after which the reaction mixture was cooled down to −20 °C and $NaBH_4$ (3.0 mg, 0.1 mmol) and Pd-C (10 wt%, 3.0 mg, 28 μmol) in 0.5 mL MeOH was added. The reaction mixture was heated to 25 °C and reacted for 10 min. After 10 min the reaction mixture was filtered through a

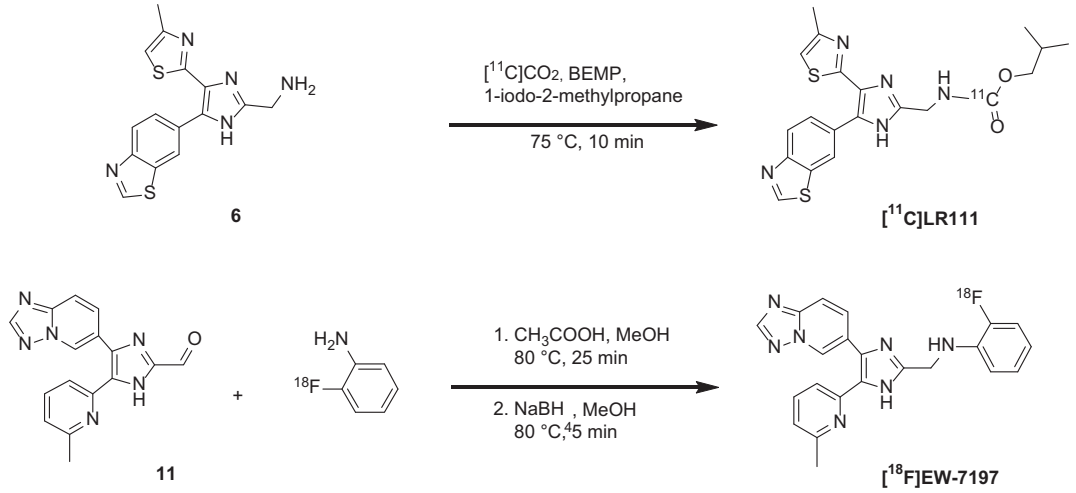

Scheme 1. Radiosynthesis of [^{11}C]LR111 and [^{18}F]EW-7197 (see Supplemental data for a detailed description of the synthesis of precursor **6**, LR111 and precursor **11**).

Millex LCR PTFE 0.45 μM 25 mm syringe filter (Millipore, Billerica, USA) into a new screw cap vial with precursor **11** (15 mg, 49 μmol) and CH_3COOH (3.0 μL, 3.2 mg, 53 μmol). This reaction mixture was heated to 80 °C and reacted for 25 min after which the reaction mixture was cooled to −20 °C. $NaBH_4$ (10 mg, 0.3 mmol) in MeOH (0.5 mL) (Fisher Scientific, Hampton, United States) was added, heated to 80 °C and reacted for 5 min. The mixture was cooled to room temperature and quenched with 1.0 mL of HPLC eluent (water/MeCN 6/4 v/v). Purification was performed by semiPREP-HPLC using an Altima C18 5 μm (10 × 250 mm) column (Grace, Breda, The Netherlands) using water/MeCN (6/4, v/v) as eluent at a flow rate of 5 mL·min^{-1}. The fraction containing the product was collected and diluted with 40 mL sterile water and passed over a tC18 SepPak cartridge (Waters, Etten-Leur, The Netherlands), pre-conditioned with 10 mL of ethanol and 10 mL of water. The cartridge was washed with 20 mL sterile water after which the product was eluted from the cartridge with 1.0 mL of sterile 96% ethanol. The ethanol was diluted to 10 vol% with formulation solution (7.09 mM NaH_2PO_4 in 0.9% NaCl, w/v in water, pH 5.2) into a sterile 20 mL capped vial (ABX, Radeberg, Germany). Analytical HPLC was performed on a Jasco (Easton, MD, USA) PU-1580 station with a Gracesmart C-18 5 μm (4.6 × 100 mm) column (Grace Alltech, Breda, The Netherlands) using water/MeCN solution (7/3, v/v) + 0.1% TFA as mobile phase, $t_R = 11.4$ min.

2.4. Development of ALK5 overexpressed and knock down A431 cells

Two independent shRNA constructs targeting ALK5 and a control non-targeting shRNA from the MISSION shRNA library (Sigma-Aldrich, St. Louis, MO) inserted in the pLKO.1-puro lentiviral vector (TRCN0000039777; Sigma-Aldrich, St. Louis, MO) were co-transfected together with VSV, GAG/POL and REV lentiviral packaging plasmid (kindly provided by Prof. Hoeben, Leiden University Medical Center) in A431 cells using polyethylenimine (MW 25 × 10^3 - Polyscience, Niles, USA). 48 h after transfection, the virus particles were harvested and filtered. Cells were seeded at a density of 2.5 × 10^6 cells per well in 12-well plates. The following day cells were transduced with the lentiviruses in a total volume of 1 mL of medium (DMEM, L-glutamine, 10% FBS, Penicillin/Streptomycine antibiotics) containing approximately 6.3 × 10^5 infective unit of virus. Following over-night incubation, the medium was refreshed and two days after transduction, selection was performed with 5 μg·mL^{-1} of puromycin. From day 14, the puromycin concentration was lowered to 2.5 μg·mL^{-1}.

2.5. Characterization of ALK expression in the A431

The expression of A431 wild type (WT), A431 ALK5 knock down (KD) and A431 ALK5 overexpressing cells, was determined with western blot analysis. A431 cells were lysed in RIPA buffer with a protease inhibitor cocktail (Sigma-Aldrich, St. Louis, MO). The cell lysates were separated by SDS-PAGE and transfected onto polyvinylideenfluoride membranes (Millipore, Burlington, USA). After protein transfer, the membranes were incubated with anti-ALK5 (SC-398; Santa-Cruz, Dallas, USA) and fluorescently conjugated secondary antibody anti-rabbit-HRO (7074; Cell Signaling, Danvers, United States). After this the membranes were incubated with Clarity ECL Substrate (1705061, Bio-Rad, Hercules, United States) and followed by scanning using light sensitive new RX medical 20 × 40 CM films (Fuji, Tokyo, Japan).

The efficiency of shRNA mediated knock down of A431 was determined with quantitative PCR. mRNA was isolated using the NucleoSpin RNA kit (Machery Nagels, Düren, Germany). cDNA was obtained with the RevertAid H minus first strand cDNA synthesis Kit (ThermoFisher scientific, Waltham, United States) and detected using the GoTaq qPCR mastermix 2x (A6002, Bio-Rad, Hercules, USA) according to the manufacturer's instructions. Quantitative PCR was performed using the CFX connect (Bio-Rad, Hercules, USA) and the following primers: *ALK5* forward: ACGGCGTTACAGTGTTTCTG, *ALK5* reverse: GCACATACAAACGGCCTATCT. As control *HPRT* forward: CTGGCGTCGTGATTAGTGAT and *HPRT* reverse: CTCGAGCAAGACGTTCAGTC were used Q-PCR relative quantification was realized by calculating the ratio of the protein expression of interest over the housekeeping gene *hypoxanthine phosphoribosyl transferase* (HPRT) mRNA expression.

2.6. In vitro cell assay with [^{11}C]LR111 in A431 cells

A431 WT, A431 ALK5 knock down (KD) and A431 ALK5 overexpressing cells (1 · 10^6 cells per well) were plated in triplicate on 6 well plates (VWR, Radnor, United States) two days prior to each experiment. On the day of an experiment the medium was replaced by fresh media with or without ALK4/5/7 kinase inhibitor SB431542 (50 μM, 0.1 μmol) [18]. After 30 min, [^{11}C]LR111 in media (1.0 mL, 1.0 MBq) was added with or without SB431542 (50 μM, 0.1 μmol, 1.0 mL). Cells were incubated at 37 °C for 30 min and the supernatant was removed. The plates were washed 3 times with phosphate buffered saline (PBS) (0.5 mL). Cells were dissolved in 10% SDS solution (0.5 mL) and pipetted into binding assay tubes, then washed with additional 250 μL and added to the tubes. All tubes were counted using a gamma well counter and stored at −20 °C until further evaluation of the protein content of the

cells. Protein content of the cells was determined using the Pierce™ BCA Protein Assay Kit (ThermoFisher scientific, Waltham, United States). All experiments were carried out three times. The uptake of the tracer (fmol·mg^{-1}) for the baseline conditions of the WT cells was normalised to 1 and the uptake in KD and overexpressed cells was expressed relative to this. Statistical analysis was performed using Graphpad PRISM (v 5.02, Graphpad Software Inc.). Tracer uptake was compared between cells with and without co-administrated SB431542 using a one-tailed unpaired *t*-test. Differences were considered significant if $p < 0.05$.

2.7. In vitro cell assay with [^{18}F]EW-7197 in A431 cells

The *In vitro cell* assay with [^{18}F]EW-7197 was conducted in the same manner as in paragraph 2.5. During the assay some minor changes were applied, listed below. All the cells ($0.5 \cdot 10^6$ cells per well) were plated in triplicate on 12 well plates (VWR, Radnor, United States). [^{18}F]EW-7197 (0.5 mL, 0.3 MBq) in media was used in the experiment. Cells were also incubated at 37 °C for 60 min. Plates were washed 3 times with PBS (125 μL). Cells were dissolved in 10% SDS solution, first in 250 μL, which was followed by another 125 μL.

2.8. In vitro assay with [^{11}C]LR111 and [^{18}F]EW-7197 in MDA-MB-231 cells

The *In vitro cell* assay with the MDA-MB-231 cells was conducted in the same manner as in paragraph 2.5. During the assay some minor changes were applied, listed below. MDA-MB-231 cells ($1 \cdot 10^6$) were plated in triplicate on 12 well plates (VWR, Radnor, United States) two days prior to each experiment. On the day of an experiment the medium was replaced with media with or without (50 μM, 50 nmol, 1.0 mL) SB431542 or (43 μM, 43 nmol, 1.0 mL) LY2157299 (Selleckchem, Houston, USA) [19]. After 30 min [^{11}C]LR111 (1.0 mL, 1.0 MBq) or [^{18}F]EW-7197 (1.0 mL, 0.3 MBq) in media was added with or without SB431542 (50 μM, 50 nmol) or (28 μM, 28 nmol) LY2157299. Cells were incubated at 37 °C for 60 min and the supernatant was removed.

2.9. Metabolite analysis in SCID mice

The metabolite analysis was carried out in healthy female SCID mice NOD.CB17-*Prkdc*^{scid}/NCrHsd (20–25 g, Charles River, Sulzfeld, Germany). Mice were injected with 21 ± 15 MBq of [^{11}C]LR111 or 14 ± 5 MBq [^{18}F]EW-7197 *via* the tail vein under isoflurane anaesthesia (2% in O_2 at 1 L·min^{-1}). At 15 and 45 min post injection (p.i.) (n = 4 per time point). Blood was withdrawn *via* heart puncture (~1.5 mL), collected in a heparin coated tube and centrifuged at 5000 rpm to separate plasma from blood cells (Hettich universal 32, Andreas Hettich GmbH & Co. KG, Tuttlingen, Germany). Solid phase extraction (SPE) cartridges (tC2, Waters, Etten-Leur, The Netherlands) were preconditioned by washing with 6 mL MeOH and 2 × 6 mL H_2O. Plasma (1 mL) was mixed with 6.0 M HCl (50 μL) and loaded onto the SPE cartridge (>99% recovery). The polar metabolite fraction was obtained by eluting the SPE cartridge with H_2O (3 mL), the non-polar fraction by subsequent elution with MeOH (2 mL) and H_2O (1 mL). The non-polar SPE fraction was injected in the HPLC. The eluate of the HPLC was collected fractionized. The fractions were counted for radioactivity using the γ-counter. The percentage of intact tracer in the non-polar fraction was determined by online HPLC analysis using a Gemini C18 column (5 μm, 10 × 250 mm, Phenomenex, Torrance, CA, USA) with a mixture of MeCN (A) and 0.1% trifluoroacetic (TFA) in water (B) as eluent according to the following scheme 0 min: 90% B; 12 min 15% B; 8 min 90% B at 3.5 mL·min^{-1} [^{11}C]LR111 R_t = 10.5 min and [^{18}F]EW-7197 R_t = 9.2 min. Results are expressed as percentage of intact tracer, polar metabolites and non-polar metabolites ± SEM (n = 4 for each time-point).

2.10. LC-MS/MS analysis of [^{11}C]LR111 in SCID mice

The mobile phase consisted of a mixture of MeCN (A) and 0.1% formic acid in water (B) according to the following scheme: 0 min 80% B, 80–20% B in 2.8 min, 20% B for 1.2 min, 20–80% B in 0.1 min, 80% B for 0.9 min. Mass spectrometer (MS) parameters: capillary potential 4500 V, source temperature 100 °C, and desolvation temperature 750 °C. Two scan functions were performed using these conditions: product ion scan of LR111 to determine high intensity mass fragment **12** and **13** (Scheme 2) and multi reaction monitoring mode (MRM) Q1 (quadrupole 1) and Q3 (quadrupole 3) were set at: 428 and 311 and 428 and 159 for parent analysis and 444 and 311 for metabolite analysis, respectively. In the MRM mode, Q1 only allows the product ion into the collision cell where they are dissociated. Q3 is fixed on a mass of one of the fragment ions. In this mode only ions that meet both the product ion and the fragment ion mass requirements are detected (Scheme 3).

[^{11}C]LR111 (10–20 MBq) was injected in the tail vein of three SCID mice and one of them received an additional 50 μg of reference compound LR111 (Scheme 2). Blood was collected after 15, 45 and 60 min p.i. and pre-treated in the same manner as written down in paragraph 2.8. The SPE (MeOH) fractions were injected into the LC-MS/MS in MRM mode. Additionally, the SPE (MeOH) fraction, blood collected after 45 min, was injected into the HPLC (method described in 2.8). The eluate of the HPLC was collected fractionized. Fractions 19 to 22 were also injected into the LC-MS/MS in MRM mode.

2.11. MDA-MB-231 tumour xenograft model and PET imaging

Female SCID mice NOD.CB17-*Prkdc*^{scid}/NCrHsd (8 weeks at arrival, 20–25 g, Charles River, Sulzfeld, Germany (n = 30)) were injected subcutaneously in the right and left flank with MDA-MB-231 cell (5×10^6 cells per flank (n = 48)) or 1×10^6 cells of the A431 cell line in the right (A431 overexpressed cells (n = 6)) and left (A431 KD cells (n = 6)) flanks. PET scans were performed on MDA-MB-231 xenografts in SCID mice (n = 4). Mice were anaesthetized with 4% and 2% isoflurane in 1 L·min^{-1} oxygen for induction and maintenance, respectively. Each mouse was positioned on the scanner bed and the respiratory rate was monitored for the duration of the experiment, adjusting anaesthesia when required. Each mouse was injected with either 11 ± 1 MBq [^{11}C]LR111 or 9 ± 1 MBq [^{18}F]EW-7197 *via* a bolus injection in the retro-orbital vein. After tracer injection, a dynamic PET scan was acquired for 60 min using either a NanoPET/CT or a NanoPET/MRI 1 T scanner (Mediso, Budapest, Hungary). After the baseline scan all animals received SB431542 or LY2157299. SB431542 (0.4 mg per mouse) was dissolved in 2% DMSO, 30% polyethylene glycol (PEG) and 68% water for injection. LY2157299 (0.5 mg per mouse, Selleck Chem, Houston, USA) was dissolved in 6 mg·mL^{-1} with 2% DMSO, 30% PEG and 68% water for injection. The blocking doses SB431542 (20 mg·kg^{-1}) and LY2157299 (25 mg·kg^{-1}) were injected intraperitoneally 30 min prior to tracer injection. The blocking scan was performed 4 h after the baseline scan for [^{11}C]LR111 and the next day for [^{18}F]EW-7197. Positron emission scans were acquired in list mode and rebinned into the following frame sequence: 4 × 5 s, 4 × 10 s, 2 × 30 s, 3 × 60 s, 2 × 300 s, 1 × 600 s, 1 × 900 s, 1 × 1200 s. The scans were reconstructed with a spatial resolution of 0.4 mm and were corrected for attenuation and scatter. Images were analysed using the freely available software AMIDE version 1.0.4 (http://amide.sourceforge.net/). ROIs were drawn in the viable part of the tumour and in the heart. The results are expressed as standard uptake values (SUV). Error bars indicate standard deviation. Statistical analysis was performed using Graphpad PRISM (v 5.02, Graphpad Software Inc.). The tumour/blood ratios were compared to the tumour/blood ratios in the blocking experiment with a one-tailed unpaired *t*-test. Differences were considered significant if $p < 0.05$. Static reconstruction was performed on the full scan time (0–60 min). Than representative PET images were generated using VivoQuant 2020. After the scanning experiments, the animals were sacrificed by cervical

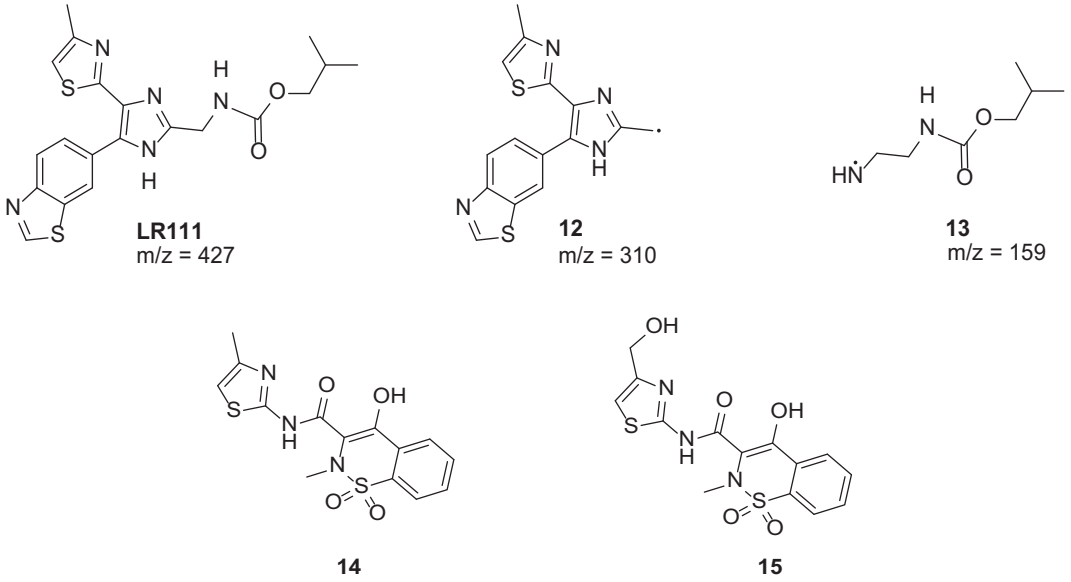

Scheme 2. Structure of intact parent LR111 and the mass fragments **12** and **13**.

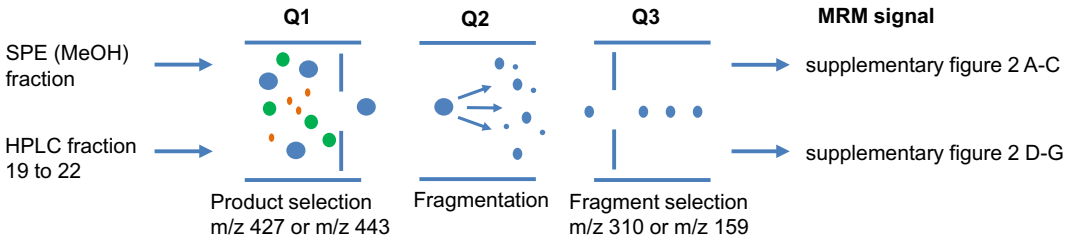

Scheme 3. Multiple reaction monitoring mass spectrometry set-up. A schematic representation of the spectrometer and injected fractions. Q1 and Q3 represent two mass filters for precursor and fragment ion selection and Q2 creates fragments *via* collisional-induced dissociation.

dislocation. The tumours were isolated and stored at −80 °C until further use.

2.12. In vitro immunohistochemistry on MDA-MB-231 tumour sections

Tumour (10 μm) sections were obtained using a Cryostat (Leica CM3050 S) and thaw mounted on Thermo Scientific Superfrost plus adhesion slides. These sections were stored at −20 °C until further handling. Frozen MDA-MB-231 tumour sections were fixed in cold acetone (−20 °C) for 1 min, air dried for 1 h and hydrated in PBS. Endogenous peroxidase activity was removed by 20 min methanol with 0.3% H_2O_2. The sections were rehydrated before incubation with primary antibody and sections were incubated overnight at 4 °C with primary antibodies directed against ALK5 (1:1000 dilution; SantaCruz, Dallas, USA; Cat#sc-398), Pecam-1 (M-20; 1:1000; SantaCruz, Dallas, USA; Cat#sc-1506), von-Willebrand Factor (1:1000; Abcam, Cambridge, UK) and α smooth muscle actin (1:10,000; Sigma-Aldrich, St. Louis, MO; Cat#A2547). All sections were mounted with ProLong® Gold antifade reagent (Invitrogen, Carlsbad, USA) containing 4′,6-diamidine-2′-phenylindole dihydrochloride (DAPI). For fluorescence quantification and comparison, sections were stained in a single run and images were collected in a single session with the same exposure time between different areas and different slides. Images were analysed using Caseviewer 2.3 software.

2.13. In vitro autoradiography on MDA-MB-231 tumour sections

Tissues were sectioned in 10 μm slices using a Cryostat (Leica CM3050 S) and thaw mounted on Thermo Scientific Superfrost plus adhesion slides. These sections were stored at −20 °C until further use. Tissue sections were defrosted, washed three times for 15 min with 5.0 mM Tris-HCl, pH 7.4 and dried in a cold stream of air. The sections were incubated for 30 min with 5.0 mM Tris HCl buffer (0.5 mL), pH 7.4 containing 1.0 MBq·mL^{-1} [^{11}C]LR111 or 0.5 MBq·mL^{-1} [^{18}F]EW-7197 with and without blocking agent (94 μM SB431542 or 56 μM LY2157299, respectively). Sections were washed in cold 5 mM Tris HCl buffer, pH 7.4 (three times 1 min) followed by a dip in ice cold water. Sections were dried under an air stream and exposed to a phosphor storage screen (GE Healthcare Lifescience, Eindhoven, The Netherlands) for 45 min. Screens were developed on a Typhoon FLA 7000 phosphor imager (GE Healthcare Lifescience, Eindhoven, The Netherlands) and analysed using Image Quant TL v8.1.0.0 (GE Healthcare Lifescience, Eindhoven, The Netherlands). Statistical analysis was performed using Graphpad PRISM (v 5.02, Graphpad Software Inc.). The tracer uptake in the tissues was compared to the tracer uptake co-administrated with SB431542 by using a one-tailed unpaired *t*-test. Differences were considered significant if $p < 0.05$. Adjacent tissue sections were used for the immunohistochemistry experiments and the autoradiography experiments.

3. Results

3.1. Radiosynthesis

[^{11}C]LR111 was synthesized using the so-called [^{11}C]CO_2 fixation methodology published by Hooker et al. and Wilson et al. [20,21]. Reaction conditions were modified according to Table 1. The trapping efficiency of [^{11}C]CO_2 in BEMP and 1,8-Diazabicyclo[5.4.0]undec-7-ene

Table 1
Reaction conditions for the radiosynthesis of [^{11}C]LR111. Yields were determined as percentage product in the crude reaction mixture on analytical HPLC and corrected for losses during synthesis.

Entry	Precursor	Base	Temperature (°C)	Yield (%)
1	Benzylamine	DBU	75	32
2	Compound 6	DBU	75	31 ± 18
3	Compound 6	BEMP	25	15 ± 14
4	Compound 6	BEMP	75	73 ± 4

(DBU) were near quantitative. After completion of the reaction, the mixture was purged with a helium flow of 25 mL·min^{-1} to remove unreacted [^{11}C]CO_2 from the reaction mixture. Analytical HPLC chromatograms for entry 2 and 4 showed high radiochemical yields of 77 ± 2% (entry 2) and 68 ± 0% (entry 4), respectively, based on HPLC analysis of the crude product mixture. However, more unreacted [^{11}C]CO_2 was released from the reaction mixture and trapped on the NaOH column after purging the reaction mixture with a helium flow. This resulted in a higher non-isolated yield of entry 4 (73 ± 4%) than that of entry 2 (31 ± 18%). [^{11}C]LR111 was obtained using the reaction conditions of entry 4 with high molar activity 126 ± 186 GBq·μmol^{-1} (at the end of synthesis) and in 17 ± 6% decay corrected yield. Up to 3.5 GBq was isolated after 35 min of synthesis, purification and formulation time. The obtained yield was sufficient to perform the *in vitro* and *in vivo* experiments.

[^{18}F]EW-7197 was synthesized with a reductive amination reaction that was based on a method published by Vasdev et al. [22,23]. Synthesis of [^{18}F]fluoronitrobenzene was accomplished in high radiochemical yields, *i.e.* 84 ± 9% (based on HPLC analysis of the crude product) in acetonitrile (MeCN). The synthesis of [^{18}F]fluoronitrobenzene in DMSO also resulted in a high radiochemical yield of 87 ± 7% (based on HPLC analysis of the crude product). However, the reduction of [^{18}F]fluoronitrobenzene to [^{18}F]fluoroaniline could in that case not be achieved with a one-pot procedure, but needed an extra solid phase extraction to remove DMSO. Therefore the synthesis of [^{18}F]fluoronitrobenzene was, after the method development of [^{18}F]EW-7197, only performed in MeCN. The reductive amination reaction required temperatures of at least 80 °C and resulted in radiochemical yields of 38 ± 17% (n = 8), based on HPLC analysis of the crude product. [^{18}F]EW-7197 was formulated with a solid phase extraction in saline with 10% ethanol. [^{18}F]EW-7197 was obtained with high molar activity 183 ± 126 GBq·μmol^{-1} (at the end of synthesis) and with 10 ± 5% decay corrected yield. Up to 3 GBq was isolated after 2.5 h of synthesis, purification and formulation time. The obtained yield was sufficient to perform the *in vitro* and *in vivo* experiments.

3.2. *In vitro cell uptake study*

In vitro uptake of [^{11}C]LR111 and [^{18}F]EW-7197 was determined in A431 WT, ALK5 overexpressed A431 cells, and ALK5 knock down (KD) A431 cells and the MDA-MB-231 cell line (Figs. 1D and 2). After 30 min, uptake of [^{11}C]LR111 and [^{18}F]EW-7197 in A431 ALK5 overexpressing cells was 1.3 and 1.5 times higher than in WT cell, respectively (Fig. 1A and B). At 60 min, cells incubated with [^{18}F]EW-7197 had a 2.5 fold increase in uptake in ALK5 overexpressed A431 cells compared with ALK5-WT and ALK5-KD cells (Fig. 1C). Blocking experiments were

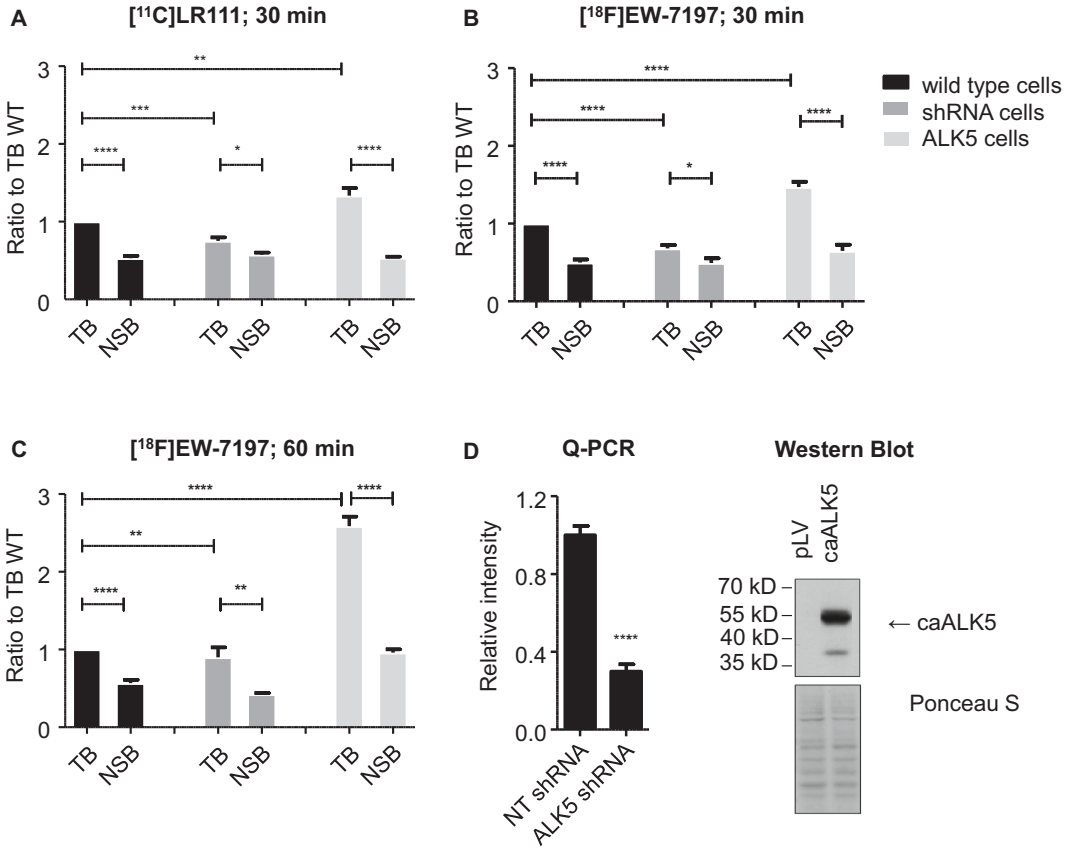

Fig. 1. Cell experiments in A431 WT, shRNA knock down (KD) and ALK5 overexpressed cells: A) incubation of [^{11}C]LR111 at total binding (TB) and following co-administration of SB431542 (non-specific binding (NSB) 50 μM) for 30 min; B) incubation of [^{18}F]EW-7197 and following co-administration SB431542 (NSB; 50 μM) for 30 min; C) incubation of [^{18}F]EW-7197 and following co-administration SB431542 (NSB; 50 μM) for 60 min; D) Q-PCR and Western blot experiments of shRNA ALK5 KD and overexpressing cells. *-symbol represents a significant difference ($p < 0.05$), **-symbol represents a significant difference ($p < 0.01$), ***-symbol represents a significant difference ($p < 0.001$), ****-symbol represents a significant difference ($p < 0.0001$).

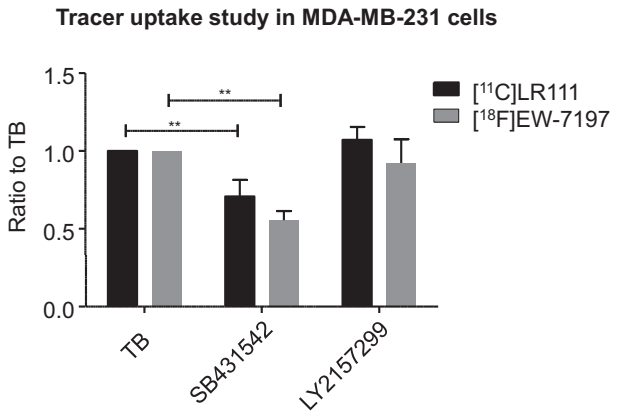

Fig. 2. Cell experiments in MDA-MB-231 cells incubate with [^{11}C]LR111 and [^{18}F]EW-7197 total binding (TB), and following co-administration of SB431542 (50 μM) and LY2157299 (43 μM) for 60 min. ** -symbol represents a significant difference ($p < 0.01$).

performed using a selective ALK4/5/7 kinase inhibitor (SB431542). Uptake of both tracers was decreased when SB431542 was added (54 ± 7% for [^{11}C]LR111 and 51 ± 5% for [^{18}F]EW-7197 in WT and overexpressed cells) showing the specificity of the tracers binding to ALK5 in the A431 cells. The Q-PCR data showed a threefold lower ALK5 expression in the KD cells compared to the A431 WT. The western blot analysis showed an increased ALK5 expression in the overexpressing cells compared to A431 WT (Fig. 1D).

Cell uptake experiments were also performed in the MDA-MB-231 cell line to determine whether selective binding of the tracers could be established in a natural expressing ALK5 cell line. SB431542 decreased uptake of [^{11}C]LR111 by 30% and that of [^{18}F]EW-7197 by 50%, both compared with non-blocked conditions (Fig. 2). LY2157299 could not diminish the uptake of the ALK5 PET tracers in the MDA-MB-231 cells.

3.3. Metabolite analysis in SCID mice with HPLC analysis

Table 2 expresses parent and metabolite fractions in percentage. After 15 min 67 ± 2% of intact [^{11}C]LR111 together with non-polar metabolites (22 ± 2%) and 10 ± 2% of polar metabolites were identified. After 45 min 39 ± 2% of intact [^{11}C]LR111 together with non-polar metabolites (24 ± 4%) and polar metabolites (35 ± 2%) were identified. [^{18}F]EW-7197 showed after 15 min, 54 ± 3% of intact tracer and 3 ± 0% of non-polar metabolites, and mainly polar metabolites (38 ± 3%) were identified. After 45 min [^{18}F]EW-7197 showed 21 ± 2% of intact tracer and 12 ± 2% of non-polar metabolites. Mainly polar metabolites (58 ± 2%) were detected.

Fig. 3A shows the radioHPLC of the non-polar fraction after 45 min p.i. In this chromatogram two non-polar metabolites and [^{11}C]LR111 were observed. Fig. 3B shows the radioHPLC of the non-polar fraction after 45 min. In this chromatogram multiple non-polar metabolites and [^{18}F]EW-7197 were observed.

Table 2
Metabolite analysis of [^{11}C]LR111 and [^{18}F]EW-7197 in SCID mice.

	[^{11}C]LR111		[^{18}F]EW-7197	
	Time p.i. 15 min	Time p.i. 45 min	Time p.i. 15 min	Time p.i. 45 min
Intact tracer (%)	67 ± 2	39 ± 2	54 ± 3	21 ± 2
Non-polar metabolites (%)	22 ± 2	24 ± 4	3 ± 0	12 ± 2
Polar metabolites (%)	10 ± 2	35 ± 2	38 ± 3	58 ± 2

3.4. LC-MS/MS metabolite characterization of [^{11}C]LR111 in SCID mice

LC-MS/MS analysis of the blood plasma collected 15 and 45 min after tracer injection revealed two metabolites with a mass of 443 m/z (Supplementary Fig. 2A–C), which corresponds to hydroxylation of the compound on two different positions with the same mass. To confirm that oxidation of the parent compound does indeed take place, an LC-MS/MS analysis was performed that could selectively detect the parent (m/z = 427) and the metabolites (m/z = 443) (Supplementary Fig. 1A–C). The following MRM transitions were used 443 m/z ➔ 310 m/z (metabolite detection) and 427 m/z ➔ 310 m/z (parent compound detection). LC-MS/MS analysis of the blood plasma from the mouse with non-radioactive compound LR111 revealed one metabolite with a mass 443 m/z. Unfortunately, metabolite concentrations in blood plasma, collected after 60 min of tracer injection, were below the measurement threshold. To confirm formation of the two metabolites, the fractions collected by HPLC were separately injected in the LC-MS/MS (Supplementary Fig. 2D–G). The first fraction contained only one hydroxylated metabolite (M1), the second fraction contained two hydroxylated metabolites (M1 and M2), the third fraction contained the other hydroxylated metabolite (M2) and the fourth fraction contained only parent tracer. The parent tracer was metabolized on the benzothiazole or methylthiazole moieties. The masses of the metabolites of [^{18}F]EW-7197 were not determined, as mainly polar metabolites were formed and the level of non-polar metabolites was below the detection limit of the LC-MS/MS.

3.5. MicroPET imaging studies in MDA-MB-231 tumour xenografts

The SCID mice which were injected with the A431 cell did not develop tumours of notable size. The SCID mice which were injected with the MDA-MB-231 cells developed tumours of 99 ± 62 mm^3 in size. Tumour to blood ratio of [^{11}C]LR111 was similar in SB431542 blocked and baseline conditions (Fig. 4A). When adding LY2157299, however, Tumour to blood ratio was reduced by 27%. Tumour to blood ratio of [^{18}F]EW-7197 could be reduced with both SB431542 (29% at 60 min) and LY2157299 (29% at 60 min) (Fig. 4B).

The standard uptake values (Fig. 4C and D) showed only blocking of LY2157299. Both tracers displayed high uptake in liver, kidneys, and bladder. The PET scans of [^{11}C]LR111 and [^{18}F]EW-7197 showed uptake into the tumour rim of the MDA-MB-231 tumour xenografts and no uptake in the core of the tumours (Fig. 5).

3.6. In vitro evaluation on MDA-MB-231 tumour sections

Expression of ALK5 was observed in MDA-MB-231 tumour sections (Fig. 6A and C). In addition, necrotic parts were observed in the core of the tumour sections (Fig. 6B). Autoradiography on MDA-MB-231 tumour sections showed high binding of both [^{11}C]LR111 and [^{18}F]EW-7197 (Fig. 6D and E). Blocking of this binding by addition of the selective ALK5 kinase inhibitors SB431542 or LY2157299 showed 50 and 40% decrease for [^{11}C]LR111 and [^{18}F]EW-7197, respectively with SB431542 being a more effective blocking agent than LY2157299 (15% more blocking of [^{11}C]LR111 and 10% more in case of [^{18}F]EW-7197).

4. Discussion

This study focused on the development of two ALK5 PET tracers and their evaluation in *in vitro* and *in vivo* models. Synthesis of both [^{11}C]LR111 and [^{18}F]EW-7197 resulted in good radiochemical yields, purities and high molar activities, making them suitable for preclinical evaluation *in vitro* and *in vivo*. As the A431 cells are easily transfectable, two A431 cell lines were generated, one with ALK5 overexpression and the other in which ALK5 was knocked down (ALK5-KD). The A431 ALK5 overexpressing cell line showed selective uptake of both tracers *in vitro*, as blocking ALK5 with SB431542 resulted in similar uptake as in ALK5-

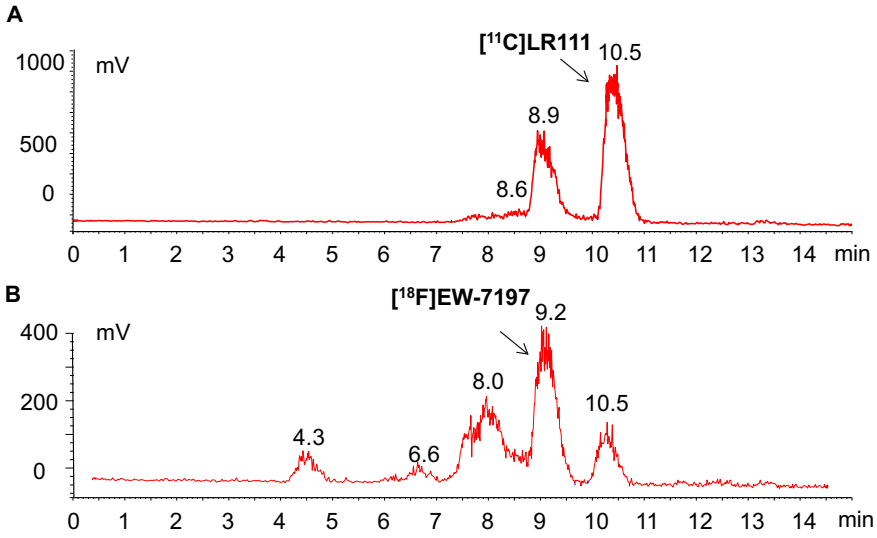

Fig. 3. Radio-HPLC chromatograms of the non-polar fraction in mouse plasma at 45 min p.i. for A) [^{11}C]LR111 and B) [^{18}F]EW-7197.

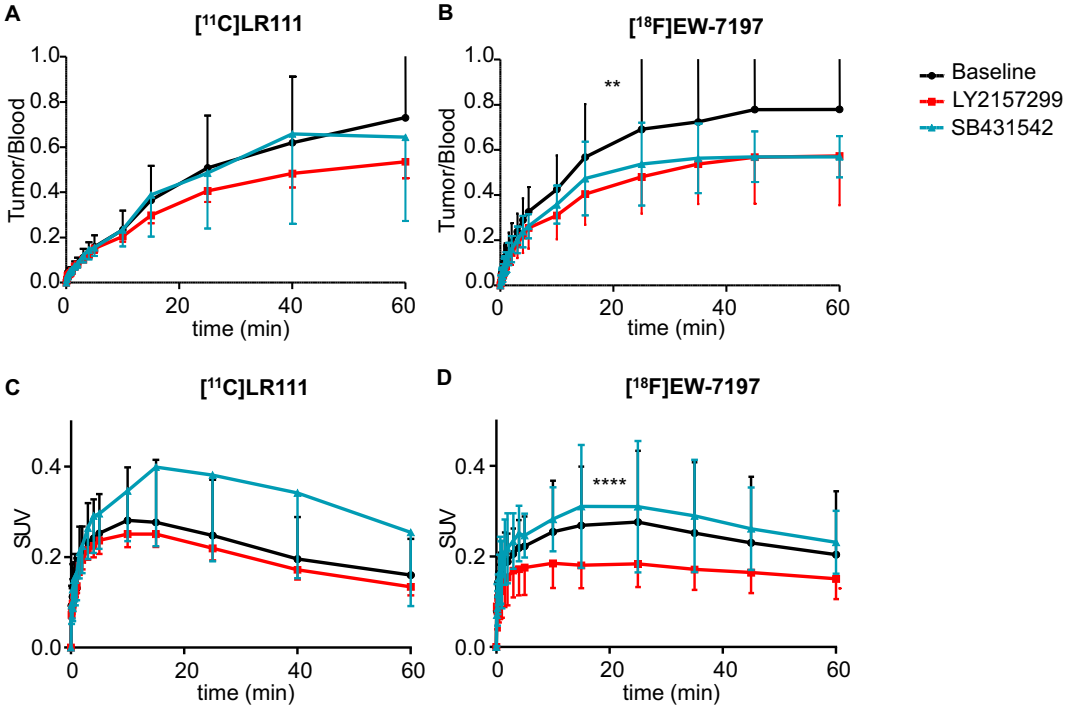

Fig. 4. Time activity curves of [^{11}C]LR111 and [^{18}F]EW-7197 in MDA-MB-231 tumours. **-symbol represents a significant difference ($p < 0.01$), ****-symbol represents a significant difference ($p < 0.0001$).

KD cells.

The stability and metabolite profiles of both tracers were assessed in healthy female SCID mice. [^{11}C]LR111 was metabolized leading to a formation of hydroxylated analogues with oxidation taking place at the benzothiazole or methylthiazole moieties. Those metabolites might bind to the binding site of ALK4, ALK5 and ALK7 as well, as some flexibility is allowed on the 2-methyl thiazole side and the benzothiazole side of the molecule that does not compromise the metabolite to bind [24]. Interestingly, a study with meloxicam showed the same outcome [25,26]. In that study meloxicam **14**, a nonsteroidal anti-inflammatory drug, was oxidised or hydrolysed by CYP2C9 and CYP3A4 in human liver microsomes towards compound **15** (Scheme 2) [25,26]. As [^{11}C]LR111 also contains a 2-methyl thiazole group, it is likely that the same happens with [^{11}C]LR111.

Metabolism of [^{18}F]EW-7197 predominantly resulted in polar metabolites and, to a lesser extent, multiple non-polar metabolites. 45 min after injection, 21 ± 2% of intact tracer was observed. The metabolites could not be identified because of the detection limit of the LC-MS/MS equipment used. As mainly polar metabolites were formed, it is unlikely that those metabolites bind to ALK4, ALK5 and ALK7.

Both tracers displayed a metabolic profile that did not prohibit ALK5 PET imaging, and they were therefore further investigated *in vivo*. Unfortunately, the preferred model of A431 tumour cells overexpressing ALK5 did not result in tumour growth in the SCID mice (only A431-KD cells did show tumour growth), resulting in a non-suitable model for ALK5 imaging. The TGFβ/ALK5 pathway is also involved in MDA-MB-

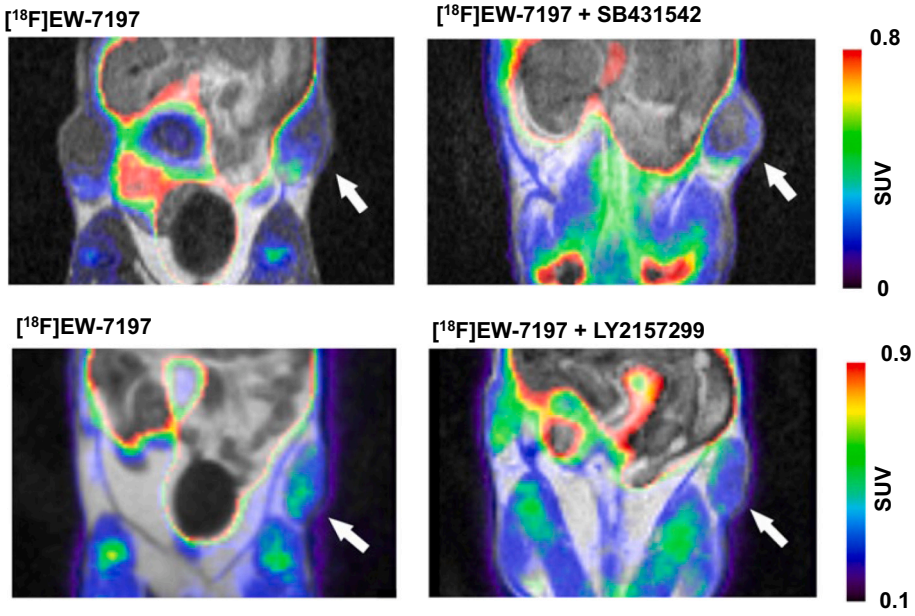

Fig. 5. Representative PET image of [^{18}F]EW-7197. The tumours are indicated by the white arrows.

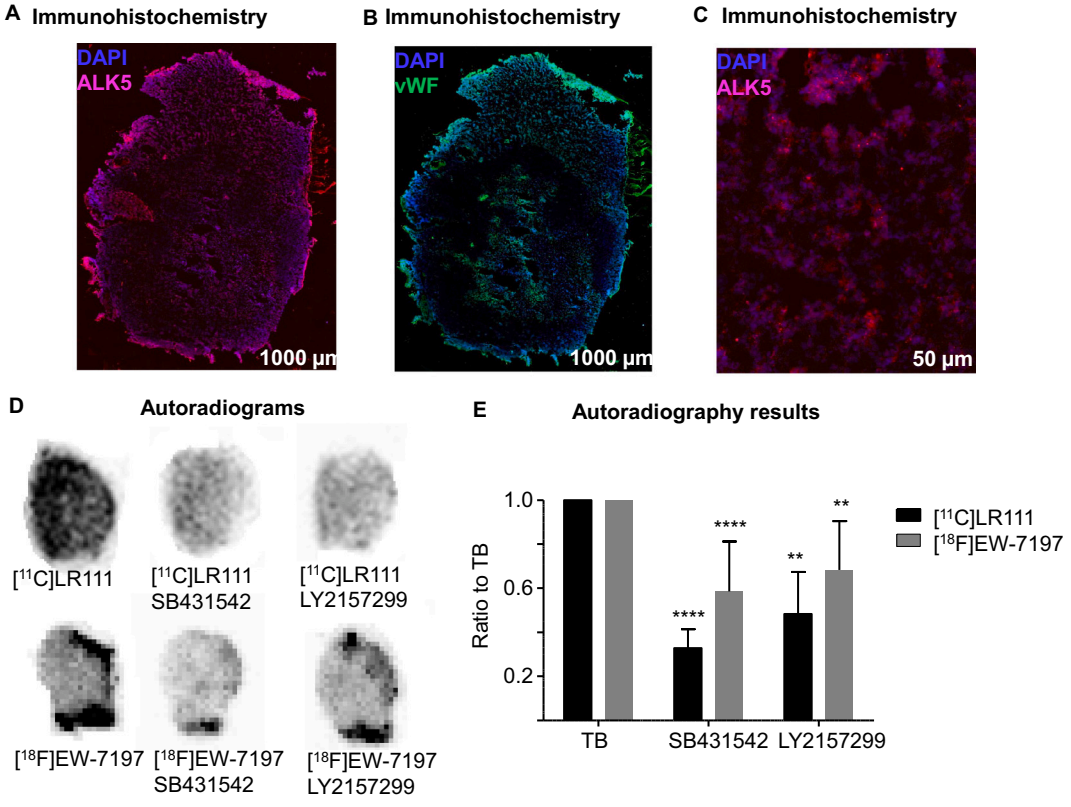

Fig. 6. A) Nuclear staining (DAPI) and ALK5 staining on MDA-MB-231tumor tissue. B) Nuclear staining (DAPI) and necrosis staining (von Willebrand factor (vWF) on MDA-MB-231tumor tissue. C) Nuclear staining (DAPI) and ALK5 staining on MDA-MB-231tumor tissue (scale bar is 50 µm). D) Representative autoradiograms of [^{11}C]LR111 and [^{18}F]EW-7197 on MDA-MB-231 tumours at total binding (TB) and under blocked conditions. E) Binding divided by total binding of [^{11}C]LR111 and [^{18}F]EW-7197 on MDA-MB-231 tumours. **-symbol represents a significant difference ($p < 0.01$), ****-symbol represents a significant difference ($p < 0.0001$).

231 cells where it causes invasive tumour growth and angiogenesis [27,28] and in a much lesser extent is ALK4 and ALK7 expressed in those tumours [29,30]. Therefore, this model was selected for further experiments, although it is known that MDA-MB-231 tumours often have necrotic cores in the xenograft models and this will affect tracer distribution in the tumour and, more importantly, potentially confound measurement of tracer uptake using PET, as the spatial resolution of PET is insufficient to distinguish between vital and necrotic tissues within a tumour.

SB431542 and LY2157299 two known ALK4, ALK5 and ALK7 kinase

inhibitor were used to confirm specificity of [^{11}C]LR111 and [^{18}F]EW-7197 in the MDA-MB-231 cell line and tumours as both compounds already showed pSmad2 or pSmad3 inhibitory potency in the MDA-MB-231 cells [29,31]. In addition, SB431542 also showed its inhibitory potency in an *in vivo* bioluminescence model in which the bioluminescence activity in the mice increased in the SB431542 mice in the first hour and reached a peak activity within 4 h post-treatment [32].

First, selectivity of both tracers was determined by using co-adding SB431542 to MDA-MB-231 cells, which contain endogenous ALK5 expression, *in vitro* [29,31]. Surprisingly, no blocking was obtained in the MDA-MB-231 cell experiment when LY2157299 was used as blocking agent. In the autoradiography experiment however, SB431542 and LY2157299 both caused significant blocking *in vitro* in which the SB431542 caused a better blocking than LY2157299. Possibly the number of cells, used in the cell experiments, was too low to cause specific blocking of LY2157299 as well.

Analysis of the PET data revealed high uptake of both tracers in liver, kidney, and bladder, which is considered normal for small molecules [33]. In the centre of the largest tumours, no uptake was observed, indicating that those tumours were indeed necrotic. Immunohistochemistry on these dissected tumours with von-Willebrand Factor (vWF) clearly showed necrotic centre with low ALK5 expression, while in the vital outer rim of the tumours ALK5 expression was high (Fig. 6A). Because of this localized expression of ALK5 within the tumours combined with the limited resolution of PET, these expression levels could not be detected separately and were averaged over the tumour, which explains the relatively low tumour to blood ratio's [^{18}F]EW-7197 (0.80 $\pm$ 0.39) and [^{11}C]LR111(0.74 $\pm$ 0.39), as assessed by PET. In this analysis we have excluded the necrotic inner core of the tumours, based on visual interpretation. As the tumour to blood ratios of [^{11}C]LR111 in the tumours was still increasing after 60 min, a longer scan time might be better. The tumour to blood ratios of [^{18}F]EW-7197 in MDA-MB-231 tumour xenografts were reduced when adding SB431542 or LY2157299, but only the tumour to blood ratio of [^{11}C]LR111 was reduced when adding LY2157299. SB431542 and LY2157299 are both moderately stable *in vivo*, with half lives of 28.5 $\pm$ 16.1 min for SB431542 in rats and 18 min for LY2157299 in mice [31,34]. Probably SB431542 or the metabolites of SB431542 interfere with the uptake of [^{11}C]LR111 in the tumours. Obviously, the results demonstrating that the new tracers selectively bind to ALK5, could not be reproduced to the same extend *in vivo*. Several reasons could be postulated for this difference, but most likely the general limitations of *in vitro* assays play an important role, as well as metabolism of the tracers and maybe even metabolism of the blocking agents. Nonetheless, overall, the results indicate that both new tracers show potential.

5. Conclusion

Two PET tracers, [^{11}C]LR111 and [^{18}F]EW-7197, were developed for imaging ALK5 expression levels and both showed low but selective uptake *in vivo* in MDA-MB-231 tumour xenografts that could be blocked by ALK5 inhibitors. Therefore, both [^{11}C]LR111 and [^{18}F]EW-7197 show promise as PET tracers for measuring ALK5 levels *in vivo*, warranting further studies in humans.

Grants

We acknowledge the support from the Netherlands CardioVascular Research Initiative; the Dutch Heart Foundation, Dutch Federation of University Medical Centres, the Netherlands Organisation for Health Research and Development and the Royal Netherlands Academy of Sciences. Peter ten Dijke is supported by Cancer Genomics Centre Netherlands. We also acknowledge support for Kondababu Kurakula by the Dutch Lung Foundation grant.

Appendix A. Supplementary data

Supplementary data to this article can be found online at https://doi.org/10.1016/j.nucmedbio.2022.05.003.

References

[1] Gordon KJ, Blobe GC. Role of transforming growth factor-beta superfamily signaling pathways in human disease. BBA-Mol Basis Dis 2008;1782:197–228.
[2] Siegel PM, Massague J. Cytostatic and apoptotic actions of TGF-beta in homeostasis and cancer. Nat Rev Cancer 2003;3:807–20.
[3] Wakefield LM, Roberts AB. TGF-beta signaling: positive and negative effects on tumorigenesis. Curr Opin Genet Dev 2002;12:22–9.
[4] Dumont N, Arteaga CL. Targeting the TGF beta signaling network in human neoplasia. Cancer Cell 2003;3:531–6.
[5] Schlingensiepen R, Goldbrunner M, Szyrach MNI, et al. Intracerebral and intrathecal infusion of the TGF-beta 2-specific antisense phosphorothioate oligonucleotide AP 12009 in rabbits and primates: toxicology and safety. Oligonucleotides 2005;15:94–104.
[6] Massague J, Blain SW, Lo RS. TGF beta signaling in growth control, cancer, and heritable disorders. Cell 2000;103:295–309.
[7] Baldwin RLR, Friess H, Yokoyama M, Lopez ME, Kobrin MS. Attenuated ALK5 receptor expression in human pancreatic cancer: correlation with resistance to growth inhibition. Int J Cancer 1996;67:283–8.
[8] Lu Yang Y, Xue T, Yuan J, Li Y, Wu Y. Increased expression of TGFbeta type I receptor in brain tissues of patients with temporal lobe epilepsy. Clin Sci 2009;117:17–22.
[9] C Medina Carlos MJ Santos-Martinez A Santana M Cristina Paz-Cabrera MJ Johnston. Transforming growth factor-beta type 1 receptor (ALK5) and Smad proteins mediate TIMP-1 and collagen synthesis in experimental intestinal fibrosis. Journal of Pathology, The.224:461-472.
[10] S Ehata Shogo A Hanyu M Fujime Y Katsuno E Fukunaga. Ki26894, a novel transforming growth factor-beta type I receptor kinase inhibitor, inhibits in vitro invasion and in vivo bone metastasis of a human breast cancer cell line. Cancer Science.98:127-133.
[11] M Thomas Matthew C Docx AM Holmes S Beach N Duggan. Activin-like kinase 5 (ALK5) mediates abnormal proliferation of vascular smooth muscle cells from patients with familial pulmonary arterial hypertension and is involved in the progression of experimental pulmonary arterial hypertension induced by monocrotaline. American Journal of Pathology, The.174:380-389.
[12] Rotteveel L, Poot AJ, Bogaard HJ, ten Dijke P, Lammertsma AA, Windhorst AD. In vivo imaging of TGF beta signalling components using positron emission tomography. Drug Discov Today 2019;24:2258–72.
[13] Amada H, Sekiguchi Y, Ono N, et al. 5-(1,3-Benzothiazol-6-yl)-4-(4-methyl-1,3-thiazol-2-yl)-1H-imidazole derivatives as potent and selective transforming growth factor-beta type I receptor inhibitors. Bioorg Med Chem 2012;20:7128–38.
[14] Jin CH, Krishnaiah M, Sreenu D, et al. Discovery of N-((4-(1,2,4 triazolo 1,5-a pyridin-6-yl)-5-(6-methylpyridin-2-yl)-1H-i midazol-2-yl)methyl)-2-fluoroaniline (EW-7197): a highly potent, selective, and orally bioavailable inhibitor of TGF-beta type I receptor kinase as cancer immunotherapeutic/antifibrotic agent. J Med Chem 2014;57:4213–38.
[15] Malek E, Kim BG, Valent J, et al. Preclinical studies and a phase I trial of the TGF-beta receptor inhibitor, vactosertib (TEW-7197), in combination with pomalidomide in patients with multiple myeloma refractory to bortezomib or lenalidomide. Blood 2018;132:4.
[16] Ryden M, Imamura T, Jornvall H, et al. A novel type I receptor serine-threonine kinase predominantly expressed in the adult central nervous system. JBiolChem 1996;271:30603–9.
[17] A complete, multipurpose, low cost, fully automated and GMP compliant radiosynthesis system. J Labelled Comp Radiopharm 2001;44:1052.
[18] Laping NJ, Grygielko E, Mathur A, et al. Inhibition of transforming growth factor (TGF)-beta 1-induced extracellular matrix with a novel inhibitor of the TGF-beta type I receptor kinase activity: SB-431542. Mol Pharmacol 2002;62:58–64.
[19] Bueno L, de Alwis DP, Pitou C, et al. Semi-mechanistic modelling of the tumour growth inhibitory effects of LY2157299, a new type I receptor TGF-beta kinase antagonist, in mice. Eur J Cancer 2008;44:142–50.
[20] Hooker JM, Reibel AT, Hill SM, Schueller MJ, Fowler JS. One-pot, direct incorporation of C-11 CO2 into carbamates. AngewChemIntEd 2009;48:3482–5.
[21] Wilson AA, Garcia A, Houle S, Vasdev N. Direct fixation of C-11 -CO2 by amines: formation of C-11-carbonyl -methylcarbamates. Org Biomol Chem 2010;8:428–32.
[22] Vasdev N, Dorff PN, Gibbs AR, et al. Synthesis of 6-acrylamido-4-(2- F-18 fluoroanilino)quinazoline: a prospective irreversible EGFR binding probe. JLabelled CompRadiopharm 2005;48:109–15.
[23] Slobbe P, Windhorst AD, Stigter-van Walsum M, et al. A comparative PET imaging study with the reversible and irreversible EGFR tyrosine kinase inhibitors C-11 erlotinib and F-18 afatinib in lung cancer-bearing mice. EJNMMI Res 2015;5:12.
[24] Amada H, Sekiguchi Y, Ono N, et al. Design, synthesis, and evaluation of novel 4-thiazolylimidazoles as inhibitors of transforming growth factor-beta type I receptor kinase. Bioorg Med Chem Lett 2012;22:2024–9.
[25] Obach RS, Kalgutkar AS, Ryder TF, Walker GS. In vitro metabolism and covalent binding of enol-carboxamide derivatives and anti-inflammatory agents sudoxicam and meloxicam: insights into the hepatotoxicity of sudoxicam. Chem Res Toxicol 2008;21:1890–9.

[26] Chesne C, Guyomard C, Guillouzo A, Schmid J, Ludwig E, Sauter T. Metabolism of meloxicam in human liver involves cytochromes P4502C9 and 3A4. Xenobiotica 1998;28:1–13.
[27] Hempel N, How T, Cooper SJ, et al. Expression of the type III TGF-beta receptor is negatively regulated by TGF-beta. Carcinogenesis 2008;29:905–12.
[28] Safina A, Vandette E, Bakin AV. ALK5 promotes tumor angiogenesis by upregulating matrix metalloproteinase-9 in tumor cells. Oncogene 2007;26:2407–22.
[29] Boldbaatar A, Lee S, Han S, et al. Eupatolide inhibits the TGF-beta 1-induced migration of breast cancer cells via downregulation of SMAD3 phosphorylation and transcriptional repression of ALK5. Oncol Lett 2017;14:6031–9.
[30] Quail DF, Zhang GH, Walsh LA, et al. Embryonic morphogen nodal promotes breast cancer growth and progression. Plos One 2012;7:12.
[31] Petersen M, Thorikay M, Deckers M, et al. Oral administration of GW788388, an inhibitor of TGF-beta type I and II receptor kinases, decreases renal fibrosis. Kidney Int 2008;73:705–15.
[32] Nyati S, Schinske K, Ray D, Nyati M, Ross BD, Rehemtulla A. Molecular imaging of TGF beta-induced Smad2/3 phosphorylation reveals a role for receptor tyrosine kinases in modulating TGF beta signaling. Clin Cancer Res 2011;17:7424–39.
[33] Giacomini KM, Huang SM, Tweedie DJ, et al. Membrane transporters in drug development. Nat Rev Drug Discov 2010;9:215–36.
[34] Herbertz Stephan S, Sawyer JS, Stauber AJ, Gueorguieva I, Driscoll KE. Clinical development of galunisertib (LY2157299 monohydrate), a small molecule inhibitor of transforming growth factor-beta signaling pathway. Drug Des DevTher 2015;9:4479–99.